International Journal of Navigation and Port Research
Vol.28, No.2 pp. 141~148, 2004 (ISSN-1598-5725)

# Observation of bubble dynamics under water in high-magnetic fields using a high-speed video camera

*Seung-Hwan Lee* · Minoru Takeda***

**Pohang Superconductivity Center, POSTECH, Pohang, Korea*
***Faculty of Maritime Sciences, Kobe University, Kobe, Japan*

**Abstract** : *The observations of rapid motion of bubbles under water for approximately 50 ms or less in high-magnetic fields of 10 T have been carried out successfully for the first time. The observation system constructed is composed of a high-speed video camera, a telescope, a cryostat with a split-type superconducting magnet, a light source, a mirror and a transparent sample cell. Using this system, the influence of magnetic field on the path and shape of single bubbles of $O_2$ (paramagnetism) and $N_2$ (diamagnetism) has been examined carefully. Experimental values describing the path are in good agreement with theoretical values calculated on the basis of the magneto-Archimedes effect, despite the effect of magnetism on the bubble. However, no effect of magnetism on the shape of the bubble is observed. In addition, the influence of magnetic field on drag coefficient of the bubble is discussed.*

**Key words** : *Bubble dynamics, Water, Magnetic field, Magnetism*

## 1. Introduction

New research and development efforts in areas such as electromagnetic ships(Nishigaki et al., 2000) ocean current electric power generator and magnetic separation from oil-contaminated seawater(Nishigaki et al., 2002) are being carried out in the context of applying magnetohydrodynamic (MHD) effects to marine science and engineering. In the applied studies of MHD effects, electricity is conducted directly through seawater, and electrolytic products such as bubbles are generated between electrodes. These products reduce the propulsion efficiency of electromagnetic ships and the efficiency of magnetic separation. However, the detailed cause of the reduction of efficiencies has not been clarified; there has also been no report on the direct observation of the behavior of bubbles in high magnetic fields.

Recently, it has been reported that water droplets can levitate and stay steadily suspended in a magnetic field (magneto-Archimedes buoyancy(Ikezoe et al., 1998), if one uses the difference in the magnetic susceptibility between water, which is diamagnetic, and the paramagnetic gas surrounding the water (compressed air or compressed oxygen). A study has reported the effects of magnetic field on the convection generated inside a water droplet falling in a magnetic field(Fujita et al., 2002). However, to the best of our knowledge, no report has appeared which discuss the effects of magnetic fields on motion of bubbles under water, or in particular, the effect of magnetic fields on the transient high-speed motion of bubbles.

In this study, we observed the motion of bubbles under water in a high magnetic field using a high-speed video camera and the effects of a magnetic field on the paths and shapes of bubbles in the context of basic research on MHD effects. We first constructed an optical observation system to investigate the high-speed motion of bubbles under water in a magnetic field generated by 10 T class superconducting magnets. We then observed the motion of a single bubble using the system and compared the results obtained by image analysis with those obtained from calculations. In the experiment, we used two types of samples with different magnetic properties, i.e., oxygen gas (paramagnetism) and nitrogen gas (diamagnetism), and discussed the difference in motion between gas bubbles with different magnetic properties.

## 2. Theory

### 2.1 Effect of magnetic fields on bubble motion

Figure 1 shows a dynamic model of bubbles under water in a magnetic field. In a zero magnetic field, the buoyancy $F_b$ [N] works on the bubble, causing it to move in the vertical ($y$) direction. Using the difference in the density between the bubble and water $\Delta\rho$ [kg/m$^3$], gravitational acceleration $g$ [m/s$^2$] and bubble volume $V$ [m$^3$], the buoyancy is given as

$$F_b = \Delta\rho g V \tag{1}$$

* Corresponding Author : Seung-Hwan Lee, rokkolsh@postech.ac.kr 054)279-5848

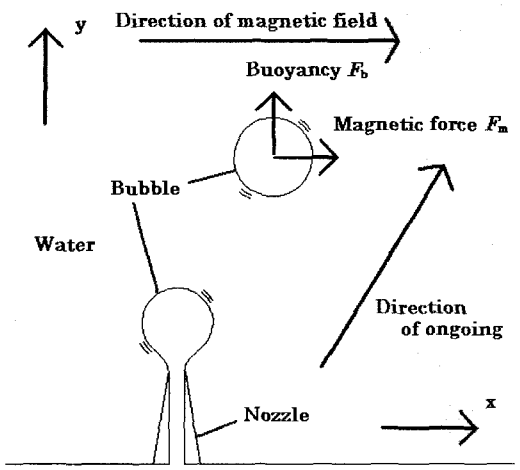


Fig. 1 Kinetic model of a bubble under water in a magnetic field

In contrast, when a magnetic field is applied in the $x$ direction, a magnetic force $F_m$ [N] is applied to the bubble under water in addition to buoyancy. The magnetic force is proportional to the difference in magnetic susceptibility between the bubble and water ($\Delta\chi$), the product of the magnetic field $B$ [T] and the field gradient $dB/dx$ [T/m] (called the magnetic force field), and bubble volume $V$ [$m^3$], and is given by

$$F_m = \frac{\Delta\chi}{\mu_0} B \frac{dB}{dx} V, \tag{2}$$

where $\mu_0$ [H/m] is the magnetic permeability in vacuum, and $\Delta\chi = \chi_G - \chi_L$ is the difference in magnetic susceptibilities ($\chi_G$: magnetic susceptibility of the bubble, $\chi_L$: magnetic susceptibility of water). Buoyancy (eq. (1)) is proportional to $\Delta\rho$; however, magnetic force (eq. (2)) is proportional to $\Delta\chi$. Eq. (2) is known to define the magneto-Archimedes effect(Ikezoe et al., 1998). As shown in Fig. 1, when there is a magnetic gradient only in the direction of the magnetic field, the bubble generated from the nozzle experiences a force in the direction of the combined buoyancy force and magnetic force; it does not ascend vertically but ascends at an angle equivalent to $F_b/F_m$, which is constant. According to the ratio of eq. (1) to eq. (2), the gradient is influenced by the difference in magnetic susceptibilities and the magnetic force field but is independent of bubble volume.

### 2.2 Effect of magnetic field on bubble shape

Let us assume that the bubble is a sphere of radius $R$ [m]. We consider the condition at the bubble boundary under a uniform magnetic field, the strength of which is $H$ [A/m], on the basis of boundary conditions for magnetic fluids(Rosensweig, 1985). Denoting the internal and external pressures on the bubble boundary as $P_G$ [Pa] and $P_L$ [Pa], respectively, the interfacial tension as $\sigma$ [N/m], and the angle between the normal line to the boundary and magnetic field, the strength of which is $H$, as $\theta$ [°], then the boundary condition at the bubble boundary is given by(Takeda & Nishigaki, 1994)

$$P_L^* = P_G^* - \frac{2\sigma^*}{R^*} + \frac{\Delta\chi B^2}{2\mu_0} + \frac{\Delta\chi B^2}{2\mu_0}\cos^2\theta. \tag{3}$$

Here, the asterisk (*) indicates the value in a magnetic field. In deriving the above equation, it is assumed that the permeabilities inside and outside the bubble boundary are equal to $\mu_0$ and used eqs. (4) and (5). These assumptions hold for bubbles under water.

$$M = \chi H, \tag{4}$$

$$B = \mu_0 H, \tag{5}$$

where $M$ [A/m] is magnetization.

The third term on the right-hand side of eq. (3) indicates the expansion of the bubble, and the fourth term indicates the stretching of the bubble in the direction of the magnetic field. However, since the value of $\Delta\chi = \chi_G - \chi_L$ ($\Delta\chi = 9.04 \times 10^{-6}$ for an underwater nitrogen bubble and $\Delta\chi = 1.10 \times 10^{-5}$ for an underwater oxygen bubble) is extremely small, the values of the third and fourth terms on the right-hand side of eq. (3) are negligibly small relative to the left-hand side of the equation. Accordingly, the deformation of a bubble under water due to a magnetic field is considered to be negligible.

## 3. Experiments

### 3.1 High magnetic field generation system

In this experiment, we used a 10 T class high magnetic field generation cryostat (RHE-1012T-SP, Oxford). Split-type superconducting magnets are installed underneath the cryostat, whose cross section is shown in Fig. 2. By placing a long glass pipe (inner diameter of 34 mm, length of 240 mm) in the cryostat, a sampling space with ambient temperature is created in the direction of the bore of the magnet. In addition, the sample can be observed visually through an observation window(diameter approximately 30mm)

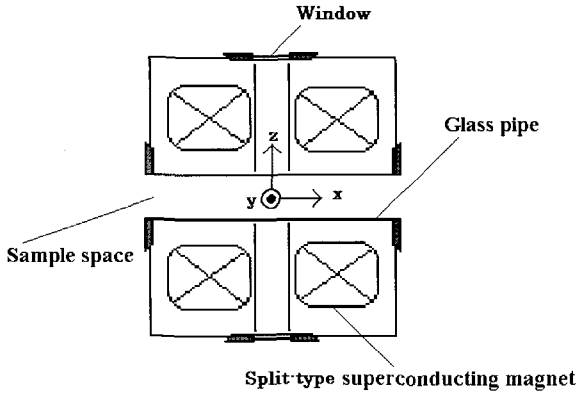


Fig. 2 Schematic diagram of horizontal cross section of the cryostat

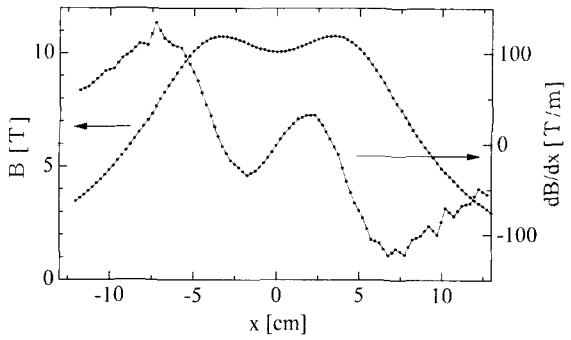


Fig. 3 Distribution of magnetic field and magnetic field gradient in the direction of $x$ axis at 10 T ($y$ = 0 cm, $z$ = 0 cm)

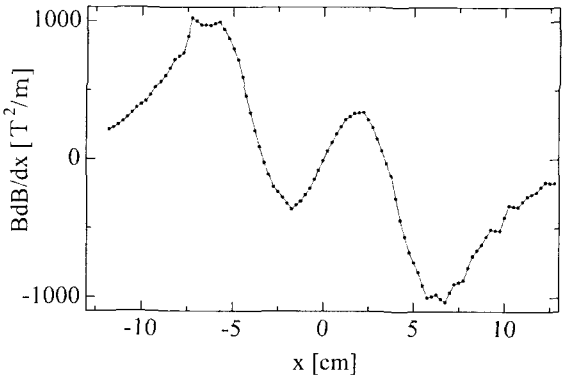


Fig. 4 Distribution of magnetic force field in the direction of $x$ axis at 10 T ($y$ = 0 cm, $z$ = 0 cm)

attached on the side. In this experiment, we designated the direction of magnetic field as the $x$ direction, and the center of the observation window (the center of the magnetic field) as the origin of the $x$, $y$ and $z$ axes (Fig. 2). Figure 3 shows the distribution of the magnetic field and magnetic field gradient observed in the $x$ axis direction. Figure 4 shows the distribution of the magnetic force field obtained from Fig. 3. According to Fig. 3, the maximum magnetic field is generated near $x$ = ±3 cm. This is characteristic of the split-type magnet.

### 3.2 Optical observation system

Figure 5 shows a horizontal cross section of the optical observation system for motion measurement in high magnetic fields. The major components of the system include a high-speed video camera (refer to next section), a telescope, a cryostat, a light source (HVC-SL, Photron), a mirror and a sample cell. Figure 6 shows a schematic of the sample cell. The observation region of the sample cell is filled with water, and the sample cell is arranged in the sample space of the cryostat. The gas line of the sample cell is connected to a gas container. To produce bubbles of different diameters, three kinds of nozzles ($\phi$ 0.6 mm, $\phi$ 1 mm and $\phi$ 2 mm) were used, and a separate sample cell was prepared for each nozzle size. The volumes of bubbles generated by these three nozzles ranged from 2.2-5.0 $mm^3$, 12-16 $mm^3$ and 29-33 $mm^3$, respectively.

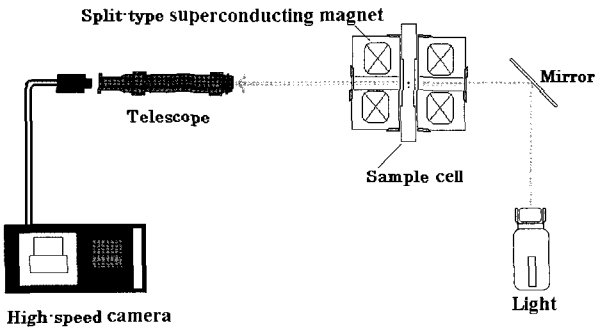


Fig. 5 Schematic diagram of horizontal cross section of the observation system

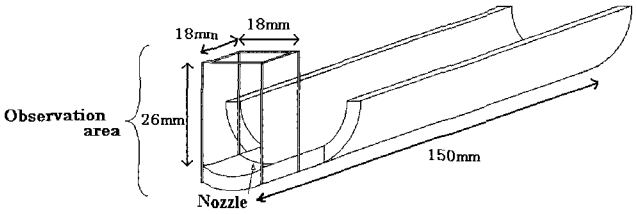


Fig. 6 Illustration of the sample cell

The light source was placed at the back of the cryostat to illuminate the sample. To easily adjust the quantity of light and incidence angle, a mirror was used to provide reflected light to the sample cell. The sample image (18 mm (vertical) × 20 mm (longitudinal) area) was magnified two-dimensionally using a telescope (approximately 8×

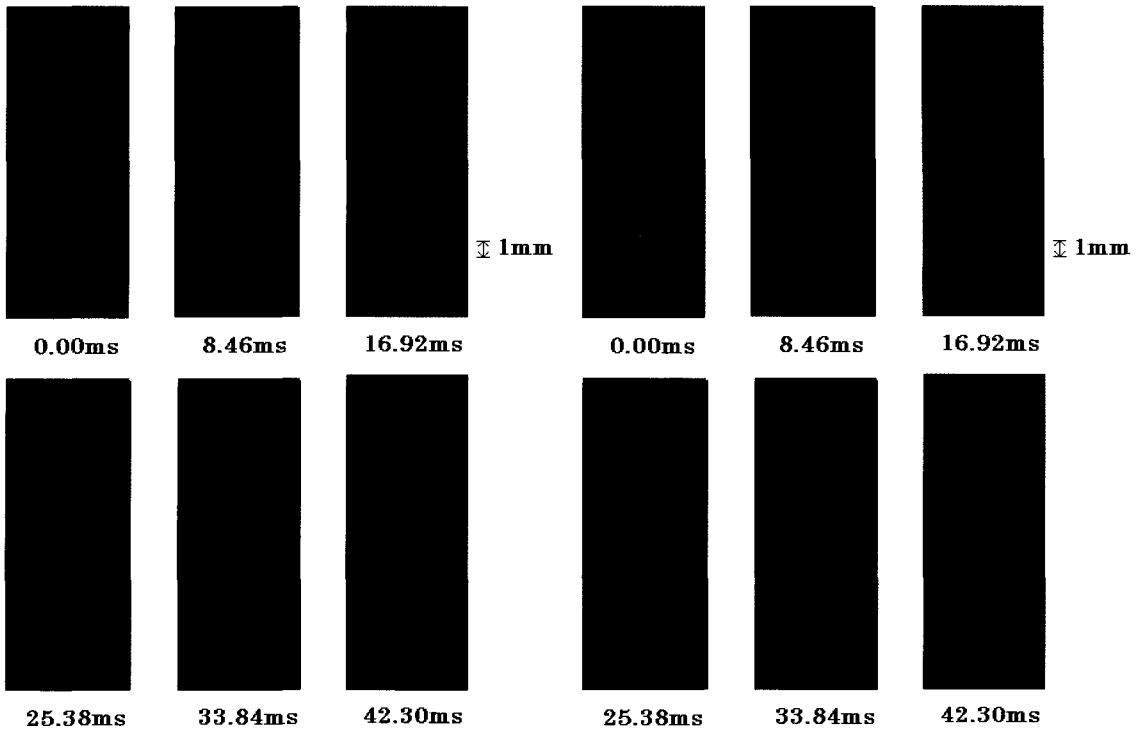


(a) $x$ = 0 cm (b) $x$ = -1 cm

Fig. 7 Obsevation of $O_2$ bubble under water in high-magnetic field of 10 T ($V$ = 31 $mm^3$)

magnification) and observed using a high-speed video camera.

### 3.3 High-speed video camera

A high-speed video camera (Speedcam 512, Weinberger) was used for the optical observations. The major components of the high-speed video camera are a central processing unit, a CCD camera, a PC monitor, a monochrome monitor and an MO drive. The resolution of the camera used in the experiment was 512 × 512 pixels (horizontal and vertical directions). The recording frequency was 1182 Hz. The imaging chip of the CCD camera consisted of a 16-block CCD; each block was fine-tuned to adjust the brightness of samples. The central processing unit contained image analysis software. The amount of shift in the $x$-axis and $y$-axis directions, velocity, acceleration and shape of the sample were analyzed using this software.

### 3.4 Experimental method

The observation direction was set along the $z$ axis, as shown in Fig. 2, and we observed the motion of the bubble along the $x$-$y$ plane. First, pure water (distilled water) was poured into the sample cell to a height of 20 mm. The nozzle was attached to the sample cell at a predesignated position in the cryostat sample space. The predesignated positions were set at three locations as follows:

(1) $x$ = 0 cm (center of the magnetic field)
Magnetic force field = approximately -11.7 $T^2/m$ (at 10 T)

(2) $x$ = 1 cm (+1 cm toward the magnetic field direction from the center of the magnetic field)
Magnetic force field = approximately 233.0 $T^2/m$ (at 10 T)

(3) $x$ = -1 cm (-1 cm toward the magnetic field direction from the center of the magnetic field)
Magnetic force field = approximately -257.6 $T^2/m$ (at 10 T).

The magnetic field was set at 0, 5, 7, 9 and 10 T at each position, and the bubble motion generated from the nozzle (oxygen gas and nitrogen gas) was observed using a high-speed video camera. Furthermore, to study the bubble shape in detail, observations were made perpendicular to the original observation direction (i.e., the $x$ direction). The purities of the oxygen gas and the nitrogen gas were 99.99% and 99.9%, respectively.

## 4. Results and Discussion

### 4.1 Image of bubbles observed

Figures 7 (a) and (b) show images of oxygen gas bubbles (the volume of 31 $mm^3$) generated at $x$ = 0 cm and -1 cm. These images were obtained approximately every 8.5 ms by setting the time at which the bubbles leave the nozzle as $t$ = 0 ms. Each box in the images corresponds to 1 mm. Figure 7 (a) shows that at $x$ = 0 cm (the center of the magnetic field) where the magnetic force field is approximately zero, a bubble moves vertically by buoyancy force only. Under this condition, the shape of the bubble is close to that of an oblate spheroid. This kind of bubble deformation was also observed under conditions of zero magnetic field. Consequently, the bubbles were not deformed by the effect of the magnetic field but by the drag received during motion in water. To confirm this, we discuss later the results of effects of a magnetic field on the bubble shape.

In contrast, as shown in Fig. 7 (b) at $x$ = -1 cm, the bubble moved in the direction of high magnetic field (toward the left-hand side in the image). Similar to the case of $x$ = 0 cm, the shape of the bubble can be approximated as an oblate spheroid with respect to its direction of motion.

### 4.2 Image analysis of bubble dynamics

Figures 8 (a) and (b) show the path of an oxygen bubble (center of gravity) using the magnetic field as its parameter on the basis of the image analysis in Figs. 7 (a) and (b). In addition, Fig. 8 (c) shows the path of the bubble generated at $x$ = 1 cm under the same conditions. The solid lines in the figures represent the gradients of the paths of ascending bubbles $\Delta y/\Delta x$ obtained by eq. (6) on the basis of eqs. (1) and (2).

$$\frac{\Delta y}{\Delta x} = \frac{F_{my} + F_b}{F_{mx}} = \frac{\frac{\Delta x}{\mu_0} B\frac{dB}{dy} + \Delta\rho g}{\frac{\Delta x}{\mu_0} B\frac{dB}{dx}}, \qquad (6)$$

where $F_{mx}$ and $F_{my}$ represent the magnetic force in the $x$ and $y$ directions, respectively. In eq. (6), we used the data on the measured magnetic field distribution and the magnetic field gradient distribution. From these figures, the gradients of the paths of ascending bubbles are close to those obtained by calculation, indicating clear dependence on the magnetic field.

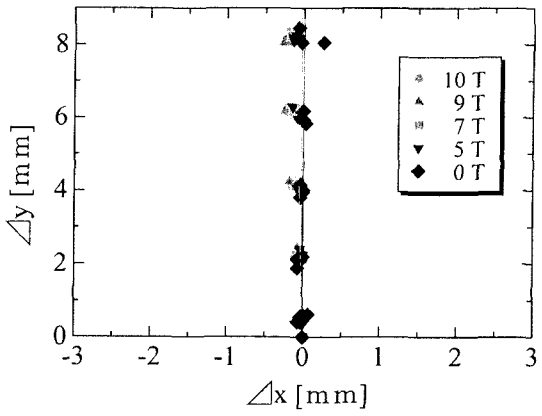


(a) $x$ = 0 cm

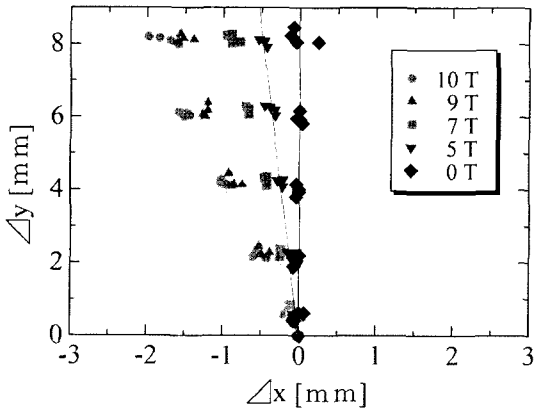


(b) $x$ = -1 cm

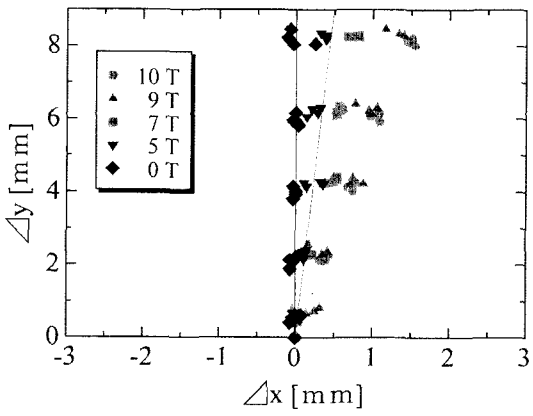


(c) $x$ = 1 cm

Fig. 8 Path of $O_2$ bubble under water as a parameter of magnetic field ( $V$= 29-33 $mm^3$)

For comparison, Figs. 9 (a) and (b) show the paths of nitrogen bubbles studied under the same conditions. These figures show that the experimentally obtained values and calculated values essentially agreed. Furthermore, these figures show that the bubbles followed very similar paths despite the differences in magnetism between oxygen and

nitrogen. This similarity can be explained by eq. (2); magneto-Archimedes effects were in action. In other words, it is understood that the magnetism (diamagnetism) of the background water rather than the magnetism of the bubble has the greatest effect on the motion of bubbles.

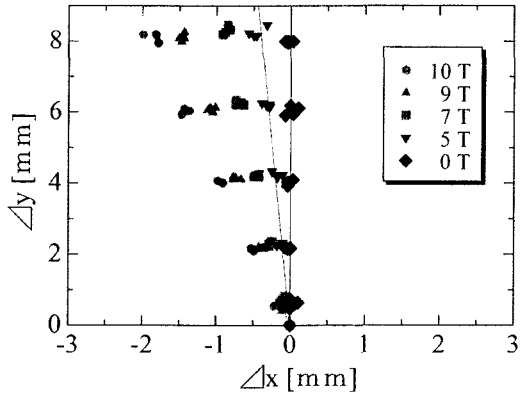


(a) $x$ = -1 cm

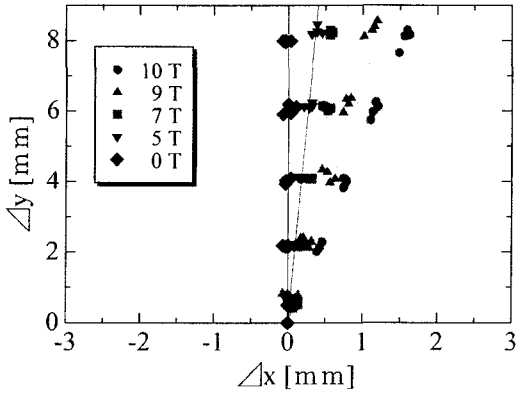


(b) $x$ = 1 cm

Fig. 9 Path of $N_2$ bubble under water as a parameter of magnetic field ( $V$= 29-33 mm$^3$)

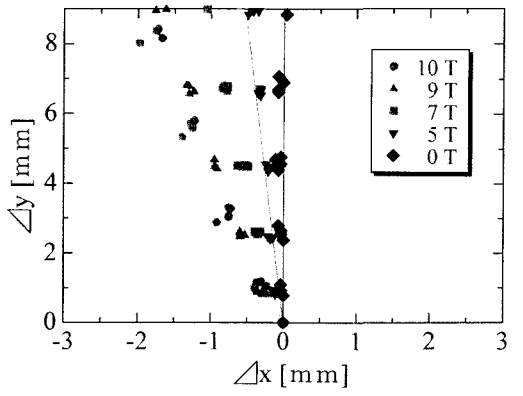


Fig. 10 Path of $O_2$ bubble under water as a parameter of magnetic field ($x$ = -1 cm, $V$= 12-16 mm$^3$)

Figure 10 shows the paths of oxygen bubbles of different volumes. The gradients of the paths of ascending bubbles roughly agree with calculated values; as shown by eq. (6), the gradient is independent of bubble volume.

### 4.3 Image analysis of bubble shape

Figures 11 (a) and (b) show bubble shape (particularly the ratio of the radius of the long axis to the radius of the short axis) as a function of time under different magnetic fields; the bubble shape is approximated as an oblate spheroid. According to these figures, the ratio increased with time from 1, and continued to increase even if it exceeded 2. This can be interpreted that the shape of the bubble moving under water deformed greatly due to flow resistance because the interfacial tension of the bubble was very small. Furthermore, we did not observe a difference in the ratio of axes caused by differences in magnetic field strength. To study the effect of magnetic field on bubble shape, we studied in detail the ratio of axes of bubbles immediately before the initiation of motion (flow resistance has no effect). Figure 12 shows the results using bubbles of different volumes. In the figure, each point represents the average of approximately five data points. Figure 12 shows that the ratio of axes remained approximately 1 and was independent of the effect of magnetic field. Furthermore, the ratio of axes was independent of bubble volume. These results were consistent with the theory described in Section 2.2.

### 4.4 Drag coefficient of bubbles

We now discuss the effect of magnetic field on the drag coefficient $C_D$ of a bubble moving under water. Denoting that acceleration, drag force and the resultant force between buoyancy and magnetic force are $a$ [m/s], $D$ [N] and $F_{mb}$ [N] respectively, a bubble moving under water in a high magnetic field satisfies the equation of motion

$$\Delta\rho Va = F_{mb} - D. \tag{7}$$

Here,

$$F_{mb} = V\left[\left(\frac{\Delta\chi}{\mu_0}B\frac{dB}{dx}\right)^2+\left(\frac{\Delta\chi}{\mu_0}B\frac{dB}{dz}\right)^2 + \left(\frac{\Delta\chi}{\mu_0}B\frac{dB}{dy}+\Delta\rho g\right)^2\right]^{\frac{1}{2}}, \tag{8}$$

and the drag coefficient $C_D$ is given by

$$C_D = \frac{2D}{\Delta\rho v^2 A}. \tag{9}$$

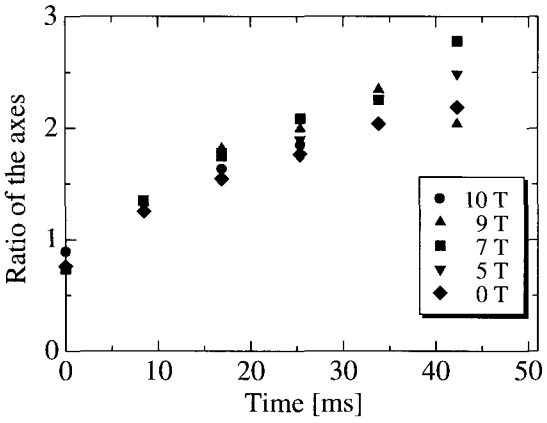


(a) $x$ = 0 cm

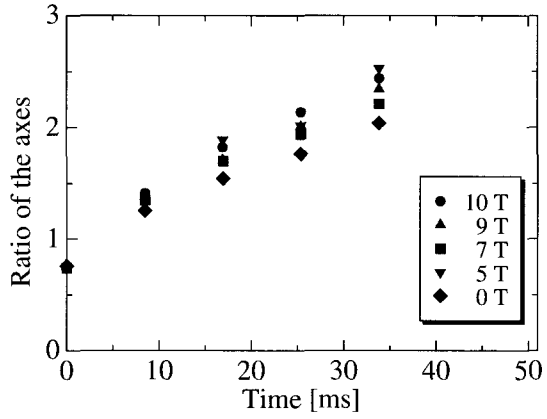


(b) $x$ = -1 cm

Fig. 11 Time dependence of ratio of the axes for $O_2$ bubble under water as a parameter of magnetic field ( $V$= 29-33 mm$^3$)

Here, v [m/s] and $A$ [m$^2$] represent the bubble velocity (center of gravity) and the maximum projected area of the bubble in the direction of motion, respectively.

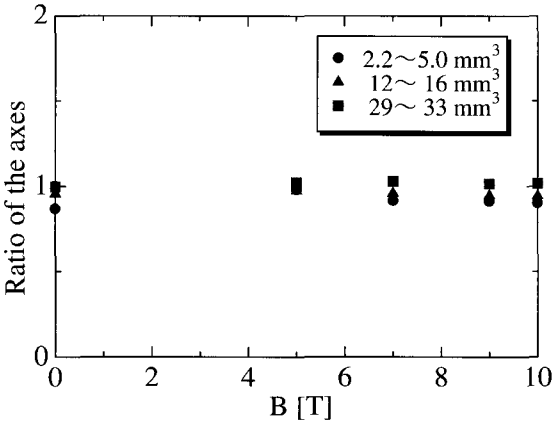


Fig. 12 Relationship between ratio of the axes of $O_2$ bubble and magnetic field as a parameter of volume ($x$ = 0 cm)

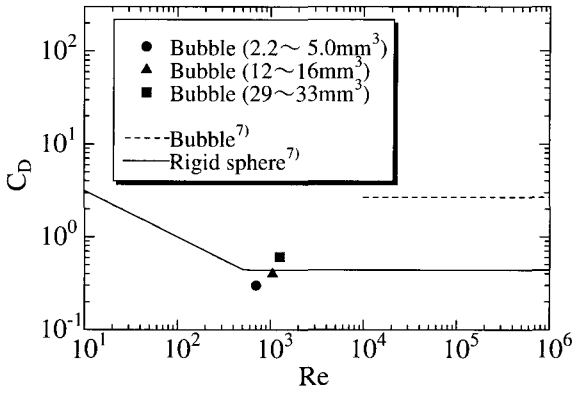


Fig. 13 Relationship between drag coefficient and Reynolds number.

We calculated the drag coefficient $C_D$ using eq. (9) after obtaining the drag force $D$ using eq. (7) on the basis of the experimental data from oxygen and nitrogen bubbles and the magnetic force field. The results show that $C_D$ decreased with time and saturated at approximately 50 ms after the start of the experiment. The values of $C_D$ varied depending on bubble volume. For example, $C_D$= 0.28 0.32 for $V$= 2.2-5.0 mm$^3$, $C_D$= 0.38-0.43 for $V$= 12-16 mm$^3$, and $C_D$= 0.59-0.63 for $V$= 29-33 mm$^3$. The value of $C_D$ was independent of the magnetic field.

In general, it is known that the drag coefficient $C_D$ is related to the Reynolds number, $R_e$(Runtai Rikigaku Handbook, 1997) Thus, we studied the relationship between $C_D$ and $R_e$ on the basis of the experimental data obtained in this study. Figure 13 shows the results. The broken line in the figure shows the value for a bubble (approximately 2.7); the solid line shows the value for a rigid sphere. As shown in Fig. 13, the $C_D$ obtained is essentially proportional to $R_e$. This result can be explained qualitatively as follows. As the Reynolds number $R_e$ increases, the drag coefficient $C_D$ increases (approaches approximately 2.7) because the bubble deforms. Conversely, if $R_e$ decreases, the bubble approaches the shape of a sphere; however, due to convection in the bubble, the friction decreases. As a result, the $C_D$ value of the bubble decreases to one that is lower than the saturation value of a rigid sphere (approximately 0.44).

## 5. Conclusions

In this study, we observed for the first time the transient high-speed motion of bubbles under water in a high

magnetic field using a high-speed video camera. By constructing an optical observation system for bubbles in a high magnetic field, we studied in detail the effects of magnetic field on the paths, shapes and drag coefficient of bubbles. The results of our study are summarized below.

(1) We were successful in monitoring the motion of bubbles for approximately 50 ms in a high magnetic field of 10 T using the observation system constructed for this study.
(2) The gradient value of ascending bubbles was dependent on magnetic field, but was independent of bubble volume, and was constant. Experimental values of the gradient essentially agreed with calculated values.
(3) With respect to the transient high-speed motion of bubbles, the paths of nitrogen and oxygen bubbles, which have different magnetic characteristics, were very similar. This phenomenon can be attributed to the magneto-Archimedes effect.
(4) The magnetic field had no effect on the shape and drag coefficient of bubbles.

## References

[1] Fujita, T., Dushkin, C. and Nakabayashi, S.(2002), Extended Abstracts (The 49th Spring Meeting), Jpn. Soc. Appl. Phys. and Related Soc. Vol.1, p.491 [In Japanese].
[2] Ikezoe, Y., Hirota, N., Nakagawa, J. and Kitazawa, K. (1998), Nature, Vol.393, pp.749-750.
[3] Nishigaki, K., Sha, C., Takeda, M., Peng, Y., Zhou, K., Yang, A., Suyama, D., Qing, Q.J., Yan, L., Kiyoshi, T. and Wada, H.(2000), Cryogenics, Vol.40, pp.353-359.
[4] Nishigaki, K., Takeda, M., Tomomori, N. and Iwata, A. (2002), Teionkougaku, Vol.37, pp.343-349 [In Japanese].
[5] Rosensweig, R.E.(1985), "Ferrohydrodynamics", Camb. Univ. Press, New York.
[6] *Ryutai Rikigaku Handbook*(1997), edited by Jpn. Soc. Fluid Dynamics, Maruzen, Tokyo [In Japanese].
[7] Takeda, M. and Nishigaki, K.(1994), J. Phys. Soc. Jpn., Vol.63, pp.1345-1350.

**Received** 10 January 2004
**Accepted** 20 March 2004